PAPER Nr. : 18

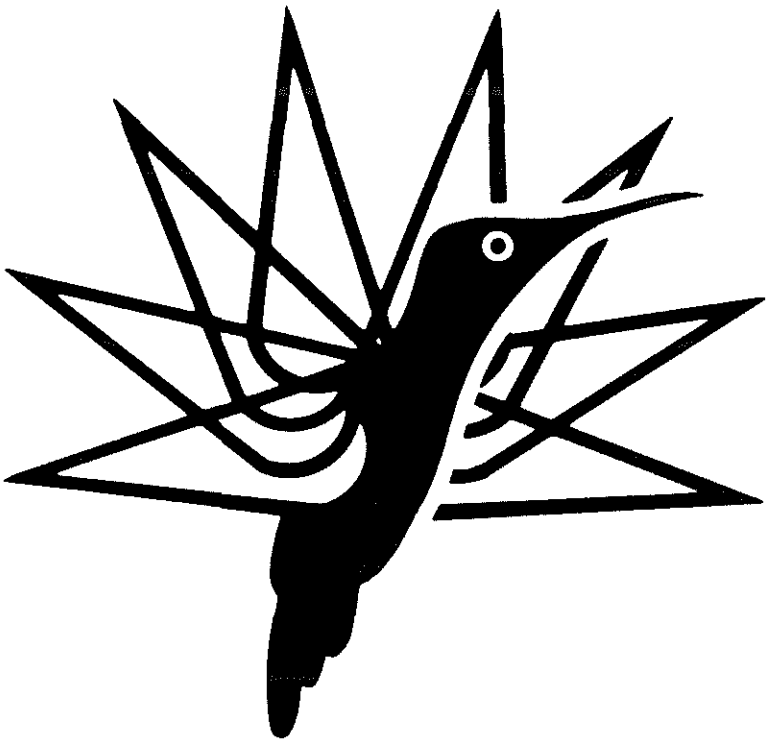

EXPERIMENTAL VERIFICATION OF AN IMPROVED ACTUATOR DISC CONCEPT

by

G.A.M. van Kuik

Stork Product Engineering

Amsterdam, the Netherlands

FIFTEENTH EUROPEAN ROTORCRAFT FORUM

SEPTEMBER 12 - 15, 1989 AMSTERDAM

EXPERIMENTAL VERIFICATION OF AN IMPROVED ACTUATOR DISC CONCEPT

by
G.A.M. van Kuik
Stork Product Engineering*
Amsterdam, the Netherlands

Summary

A study on the validity of Froude's actuator disc concept has been conducted. At the 13th Rotorcraft Forum (Van Kuik, ref. 1) a modification of the concept has been proposed in order to improve the performance prediction: the disc with a uniform, normal load should be supplemented by edge forces, acting on the edge singularity. This singularity was shown to be a vortex.
The present paper describes the validation of this concept for real rotors. First an invalid assumption in the momentum theory, based on Froude's concept, is discussed: this theory does not distinguish the total thrust and the thrust converting power, but assumes these to be identical. A proof of principle is presented that this assumption is not valid when applied to rotors. The momentum theory including edge forces avoids this assumption.
An experiment on a model rotor in hover has been performed in order to quantify the ratio of the total thrust to the thrust converting power. This ratio appeared to be 1.15; the prediction of the wake contraction using this ratio became 0.757, while .77 was the experimental value. As the classical prediction amounts 0.707, this is a significant improvement.

1 Introduction

At the 13th Rotorcraft Forum the actuator disc research at Eindhoven University of Technology was reported (Van Kuik, ref. 1). The results concerned the actuator disc itself, with emphasis on the edge singularity. This was determined to be a discrete vortex, capable of carrying an edge force depending on the velocity at the edge, see figure 1. As the edge forces are perpendicular to this velocity, they do not perform work. Therefore the momentum theory accounting for these edge forces distinguishes the total thrust, including a contribution of the edge forces, and the thrust converting power, without such a contribution.

---

*Present employment, the work described in the paper has been conducted at Eindhoven University.

In the classical momentum theory, these thrusts are assumed to be equal. The performance prediction based on the modified momentum theory shows a qualitative improvement compared with the classical one.

The present paper investigates the validity of the mentioned distinction for real rotors. First an analysis of the load on a rotor blade is presented. The second part of the paper describes an experiment on a model rotor in hover.

2 An invalid assumption in the momentum theory for rotors

The classical momentum theory, based on the disc concept of Froude, is derived for uniformly loaded discs.

The power converted to the flow by such an uniform load is $P = T\bar{U}_d$, where T is the total thrust and $\bar{U}_d$ the average velocity through the disc. If the distribution is non-uniform, $P \neq T\bar{U}_d$: T converting power is not equal to the total thrust.
The force field of a rotor does not satisfy Froude's assumption, which is illustrated by figure 2. It shows a one-bladed, flat plate, zero pitch rotor. If the angular velocity is high enough the rotor acts as a windturbine. An elementary vortex line is sketched having a spanwise as well as a chordwise component on the blade. Considering an inertial frame of reference, the forces on the vortex line perform work if they contribute to the torque. The force on the chordwise bound vorticy does not do so while it clearly has an axial component. If the pitch angle is non-zero or the aerofoil is different, the chordwise vorticity may have an axial component by which the force on it may contribute to the torque. This however does not affect the proof of concept given here.

The spanwise distribution of the chordwise vorticity depends on the geometry of the rotor; for a rectangular blade this vorticity is concentrated near the edge resulting in increased tip loads as measured by Gray etal. (ref. 2) see figure 3. The total amount of chordwise vorticity γ_c depends only on the maximum of the spanwise vorticity; as each lifting rotor experiences radial velocities v, the integrated chordwise load will always be non-zero. Inspection of the signs of γ_c and v shows that the chordwise and spanwise load have the same direction. Therefore the total thrust is always larger than the thrust converting power. This suggests that the use of the momentum theory including edge forces, which distinguishes these thrusts, should improve the performance prediction compared with the classical one.

As described in the previous paper (ref. 1), the main result of this modified momentum theory is the prediction of the average velocity through the rotor disc as $\bar{U}_d = \frac{1}{2} (U_0 + \bar{U}_\infty)\ T/T_{work}$, where T_{work} is the thrust performing work, T the total thrust, U_0 the undisturbed velocity for upstream, and $\bar{U}_\infty$ the average wake velocity for downstream. Writing R_{wake} for the fully developed wake radius, and substituting $U_0 = 0$ and $\bar{U}_d\ R^2 = \bar{U}_\infty\ R^2_{wake}$, the modified momentum theory predicts for the wake contraction of a hovering rotor

$$\frac{R^2_{wake}}{R^2} = \frac{1}{2}\ \frac{T}{T_{work}} \qquad (1)$$

If the load distribution on the spanwise and chordwise vorticity is known, the ratio T/T_{work} can be determined. A more general approach is to define T_{work} as the 'effective' thrust doing work, defined by

$$T_{work} = P/\bar{U}_d \qquad (2)$$

where P is the power converted to the flow. P,T and $\bar{U}_d$ can be measured by which the ratio T/T_{work} is known, and (1) can be verified.

3 The experiment

The aim of the experiment is to quantify the ratio T/T_{work} by measuring T with a balance, and by determining T_{work} via (2). Then this ratio is used to predict the wake contraction (1), which can be compared with the measured contraction. The power is measured in the flow: in a plane immediately downstream of the rotor the local velocity and the local increase of energy are measured, by which P can be determined. The average velocity $\bar{U}_d$ is determined by measuring the mass flow in the wake. Furthermore stroboscobic photography is used as a qualitative tool in analyzing the flow field. The model has a diameter of 1.02 m Ø , and has 2 rectangular, untwisted blades. The chord to radius ratio is 1/10. The pitch angle is 8°, the angular velocity 9 Hz. The height above the ground is 3.50 m. Figure 4 and 5 show the main measuring devices: a co-rotating rake and a traversing mechanism with two single hot wires mounted. Figure 6 shows the notations used, and the planes of measurements: A1 is the plane just downstream of the rotor: x/R = 0.03529 while A2 is at a downstream distance x/R = .5.

The rotating rake

Figure 4 shows the rake with total pressure tubes. If all tubes except a symmetric pair are closed, the local total pressure p_t (averaged on both sides) is transmitted to the fixed world by means of an air chamber at the hub. In this chamber the pressure is $p_t - \frac{1}{2}\rho(\Omega r)^2$ due to the centripetal pressure gradient in the main tubes. Using a conventional Betz manometer, this pressure is measured against the atmospheric pressure p_0, so the measured value is $p_t-(p_0 + \frac{1}{2}\rho\Omega^2r^2)$. The term between brackets is the undisturbed total pressure in the rotating system; undisturbed implies that the air is at rest in the inertial system. Writing $H = p_t$ where H is the Bernoulli constant, the rake measurements yield local values of $(H-H_0)_r$. The index r refers to the rotating system. As shown in the appendix, $(H-H_0)_r = -\rho w\Omega r$ with w the azimuthal velocity in the inertial system, see figure 5. By varying the azimuthal position of the rake and the position of the open tubes, the distribution of $(H-H_0)_r$ and w are known.
Figure 7 shows the positions of the rake data. Most data are measurement data; if the variation of $(H-H_0)_r$ is very small, the distance between the positions is increased. Interpolated data are used on the remaining grid positions. The calibration of the rake is very easy: with the rotor blades removed, the pressure difference at the manometer has to remain zero, independent of the rpm and radial position of the open tubes. Any deviation indicates leakage. The tubes have been calibrated with respect to flow misalignment. This was not felt up to 15°.
Figure 8 finally shows the distribution of $(H-H_0)_r$. The 'mountain rig' is the passage of the vortex sheet. The mountain itself, appearing as two peaks due to the graphical presentation, is the tip vortex.

The hot wire anemometry

By requiring the hot wire anemometry to be as simple as possible in order to have accurate and firm results, the wires are choosen to be relatively long (1/100 R) by which a length to diameter ratio of 1000 is obtained. Then the wires are insensitive to the flow component in wire direction which has been confirmed by calibration. By directing the wire radially (wire A in figure 6) it measures u^2+w^2; an axial wire B measures v^2+w^2.
As w is provided by the rake measurements, u and v are known at once without complex manipulation of the wire signals. The wires are located in plane A1; their radial position coincide with the rake tube positions. Wire A and B are recorded simultaneously. The signals are recorded during 27 revolutions. Only the revolutions which show a deviation of the angular velocity less than ½% are

taken into account. The number of selected revolutions appears to be 20-25. During a time interval of one revolution, 222 data are sampled. The data corresponding with the grid of figure 6 are elaborated in order to obtain local values of $|u|$ and $|v|$. The direction of the flow is not provided by the measurements. This is derived from stroboscopic smoke photography, and by requiring the change of direction to be continuous except at the tip vortex and vortex sheet passage.

Figure 9 and 10 show the distribution of u and v respectively. The data are averaged on the positions ϕ and $\phi+\pi$, so the figures are symmetrical with respect to the blade position.

A vectorial presentation is given in figure 11, for several azimulthal positions. The passage of the tip-vortex is located at $\phi = 75°$. The vectorial average velocity is shown in figure 12, where also the blade bending is given.

The wake measurements in plane A2 (x/R = .5)

At x/R = .5 the wake contraction is not completely finished: the stroboscobic smoke photo's show a final contraction ratio $R_{wake}/R \approx .77$, while at x/R = .5 this ratio is $\approx .8$. R_{wake} is defined as the radius of the tip vortex position.

The mass flow through plane A2 equals the mass flow through the rotor, by which $\bar{U}_d$ can be determined. Furthermore the measurements in this plane are used to check the momentum and energy balances.

The hot-wire denoted A in figure 6 is also used in plane A2 including the same data processing. Figure 13 shows the resulting distribution of $\sqrt{u_2^2 + w_2^2}$.

In contrast with figure 8 to 10, the data for $0 \leq \phi \leq \pi$ are not identical with the data for $\pi \leq \phi \leq 2\pi$, as no averaging has been done. The picture presents the distribution in one complete period, showing some asymmetry. This may be caused by tip vortices of slightly unequal strength. A similar picture of $\sqrt{u_1^2 + w_1^2}$ in plane A1 did not show this asymmetry.

As u_1 and w_1 are known in plane A1, a second relation between u_2 and w_2 in plane A2 is provided by determining 'average' streamtubes connecting A1 and A2:

$$\bar{u}_2(r) = \bar{u}_1(r) \frac{\overline{w}_1(r)}{\overline{w}_2(r)} \qquad (3)$$

(3) expresses the conservation of moment of momentum in a streamtube, which is defined by the conservation of mass. In such a way the azimuthally averaged value $\bar{u}_2^2 + \overline{w}_2^2$ is split up in $\bar{u}_2^2$ and $\overline{w}_2^2$ by which the mass flow is known.

The average total pressure tube is measured using a standard tube connected to a Betz manometer. As the unsteady part of the flow field does not enter the energy balance (see the appendix) these azimuthally averaged data can be used to determine the power in the wake. This serves as a check on the power determination in plane A1. As the average values of $p_t = p + \frac{1}{2}\rho\,(u_2^2 + v_2^2 + w_2^2)$ and $(u_2^2 + w_2^2)$ are known from the tube and wire measurements resp., the average static pressure p can be determined, if $\frac{1}{2}\rho v_2^2$ is neglected. As this term is expected to be very small, a global check of the axial momentum balance is possible.

4 The results of the experiment

As the air density ρ is the only parameter which is not adjustable, all measured data have been made dimensionless by the ρ at the time of measuring. In such a way the data are independent of ρ and may be compared mutually.
The power P is determined by evaluating equation (a-4):

$$\frac{1}{\rho} P = \iint u\, w\, \Omega\, r\, dA_1 = 9.381\ m^5/s^3 \tag{4}$$

v and w have not been measured for r/R<0.4. A linear interpolation of u and w towards zero of the axis is assumed. This is confirmed by measuring the kinematical average pressure using a Prandtl-Meyer tube.

The thrust is:

$$\frac{1}{\rho} T = 4.9773\ m^4/s^2 \tag{5}$$

The average velocity through the rotor disc u_d is obtained as:

$$\bar{u}_d = \iint u \frac{dA_2}{\pi R^2} = 2.16\ (m/s) \tag{6}$$

Using (2), the thrust converting power is

$$\frac{1}{\rho} T_{work} = \frac{1}{\rho} \frac{P}{\bar{u}_d} = 4.3431\ m^4/s^2 \tag{7}$$

so:

$$\frac{T}{T_{work}} = 1{,}15 \tag{8}$$

Using this ratio, (1) predicts the wake contraction to be

$$\frac{R_{wake}}{R} = 0.757 \qquad (9)$$

where the classical prediction is $\frac{1}{2}\sqrt{2} = 0.707$.
The measured wake contraction is ≈ 0.77 so (9) denotes a significant improvement of the prediction.
(8) and (9) are ratio's, so concern relative values. An absolute value of $\bar{U}_d$ can be predicted as by (1) $\bar{U}_d = \bar{U}_{\infty,classical}\ T/T_{work}$. With $\bar{U}_{\infty,classical} = \sqrt{T/2\rho\pi R^2}$, the predicted value becomes 2.005 m/s, which is 0.93 times the measured value. However, the validity of this prediction is doubtful; $\bar{U}_{\infty,classical}$ is used as reference value, obtained by a momentum theory which may be invalid.

The power measured in plane A2 is

$$\frac{1}{\rho}P = \iint u\,(H - H_o)\,dA_2 = 9.129\ m^5/s^3 \qquad (10)$$

which is ~ 2.7% lower than (7). This may be caused by loss of mechanical energy into diffusion between planes A1 and A2. The axial momentum balance

$$\iint u^2\,dA_2 = \frac{1}{\rho}T_{tot} - \frac{1}{\rho}\iint (p - p_o)\,dA_2 \qquad (11)$$

is satisfied with a deviation of 4% of the thrust. If $\frac{1}{2}\rho v_i^2$ should be accounted for (see the last alinea of the preceeding section), this deviation becomes smaller. Both data confirm that the experimental method is accurate enough.

5 Conclusions

The distinction between the total thrust and the thrust converting power appears to be significant: the effective thrust, which is the thrust doing work, is only 87% of the total thrust. Using the momentum theory which takes account of this distinction, the prediction of the wake contraction improves significantly. Furthermore a proof of principle is presented that Froude's assumption of the total thrust being equal to the thrust doing work, is incorrect if applied to rotors. This proof and the experiment lead to the final conclusion that the distinction between the total thrust and the effective thrust is necessary in the physical interpretation of rotor flow by means of momentum theory.

Acknowledgement

The research described in this paper is a part of the actuator disc research at Eindhoven University of Technology. This research was started based on the experience in using the momentum theory for windturbine development. A survey of the research is presented in ref. 3. A final report will be published, ref. 4.

References

1 G.A.M. van Kuik; The actuator disc edge singularity: the key to a revised acutaotr disc concept and momentum theory, Paper presented at the 13th European Rotorcraft Forum, 1987, Arles France.

2 R.B. Gray, H.M. McMahon, K.R. Stenoy, M.L. Hanimes; Surface pressure measurements at two tips of a model helicopter rotor in hover, NACA-CR-3281, 1980.

3 G.A.M. van Kuik; On the revision of the actuator disc momentum theory, Paper presented at the European Wind Energy Conference 1989, Glasglow.

4 G.A.M. van Kuik; On the validity of Froude's actuator disc concept, Thesis at Eindhoven University of Technology, Department of Physics, to appear at the end of 1989.

APPENDIX A: THE DETERMINATION OF THE POWER

The equation of motion in the inertial system is:

$$\underline{\nabla} H = \underline{f} + \rho \underline{v} \times \underline{\omega} - \rho \frac{\partial \underline{v}}{\partial t} \qquad (a\text{-}1)$$

Where $\underline{f}$ is the force density representing the action of the rotorblade, and $\underline{\omega}$ is the vorticity.
The power is

$$P_i = \iiint \underline{f} \cdot \underline{v} \, dG = \iiint \left[\underline{v} \cdot \underline{\nabla} H + \rho \underline{v} \cdot \frac{\partial \underline{v}}{\partial t} \right] dG \qquad (a\text{-}2)$$

where G is any volume enclosing the rotor.
Now G is choosen to be bounded by plane A1 extending to infinity (see figure 5), and a half-sphere with infinite radius. The second term can be interpreted as the time derivative of the amount of kinetical energy enclosed in G.
As the flow is periodical, the distribution of $\frac{1}{2}\rho\underline{v}.\underline{v}$ is also periodical, but the integrated amount is constant in time. Therefore (a-2) becomes, using Gauss' divergence theorem and the conservation of mass $\underline{\nabla}.\underline{v} = 0$:

$$P_i = \iint u (H - H_o) \, dA_1 \qquad (a\text{-}3)$$

An alternative way of determining P_i is to consider the increase of moment of momentum in G by the torque Q. As $P_i = Q\Omega$, the second expression for P_i is:

$$P_i = \iint \rho u w \Omega r \, dA_1 \qquad (a\text{-}4)$$

In the rotating system (index r) the velocity is

$$\underline{V} = \underline{v} - \underline{\Omega} \times \underline{r} \qquad (a\text{-}5)$$

and the equation of motion is

$$(\underline{V} \cdot \underline{\nabla}) \underline{V} + 2\underline{\Omega} \times \underline{V} + \underline{\Omega} \cdot (\underline{\Omega} \times \underline{r}) = \frac{1}{\rho} (\underline{\nabla} p + \underline{f}) \qquad (a\text{-}6)$$

which is rewritten as

$$\frac{1}{\rho} \underline{f} = \frac{1}{\rho} \underline{\nabla} \left[H_r - \frac{1}{2} \rho (\Omega r)^2 \right] - \underline{V} \times (\underline{\nabla} \times \underline{V} + 2\underline{\Omega}) \qquad (a\text{-}7)$$

where $H_r = p + \frac{1}{2}\rho\underline{V}.\underline{V}$. Introducing the undisturbed ($\underline{v} = 0$) Bernoulli constant $H_{r,0} = p_o + \frac{1}{2}\rho(\Omega r)^2$ the power in the rotating system becomes

$$P_r = \iiint \underline{f} \cdot \underline{v}\, dG = \iint u \left[H_r - H_{r,o} \right] dA_1 \qquad \text{(a-8)}$$

analogous to the derivation of (a-2). Comparison of (a-4) and (a-8) shows that only the change of H determines the relation between P_i and P_r.
Now $(H-H_o)_i = -(H-H_o)_r$: the change of H is equal but opposite in an inertial and moving system (compare the decrease of H in the wake of a 2-D aerofoil in a windtunnel with the increase of H in the wake of the same aerofoil travelling in air which is at rest far upstream).
The conclusion is that $P_r = -P_i$; comparison of (a-8) with (a-4) then gives

$$H_r - H_{r,o} = - \rho w \Omega r \qquad \text{(a-9)}$$

As discussed in section 3, the co-rotating total pressure rake measures $(H-H_o)_r$, so the rake data provide the azimuthal velocity w. With the axial component u measured by the hot wire anemometry, P_i can be determined using (a-4).

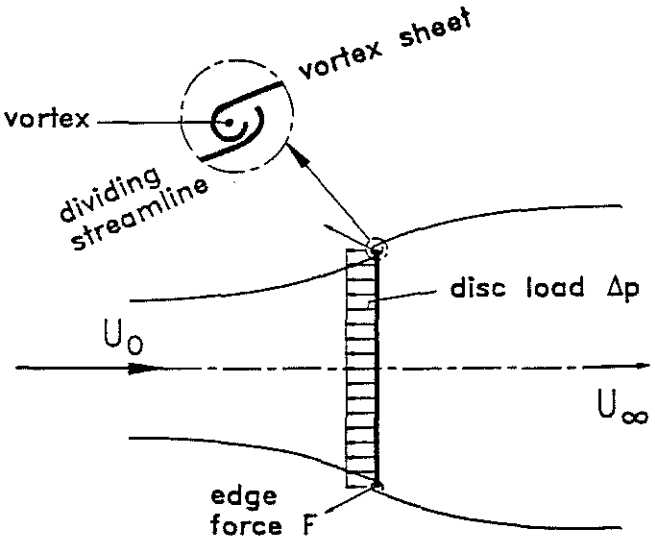

Figure 1: the modified actuator disc concept, showing a decelerating flow.

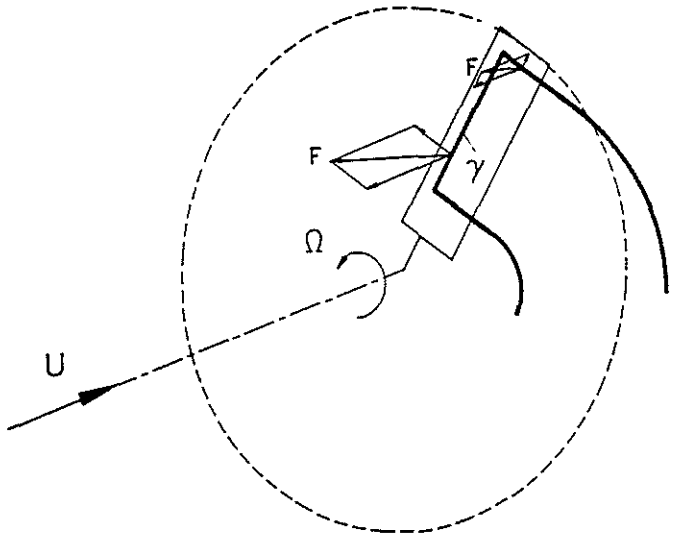

Figure 2: the load on the spanwise and chordwise bound vorticity of a zero pitch, flat plate rotor.

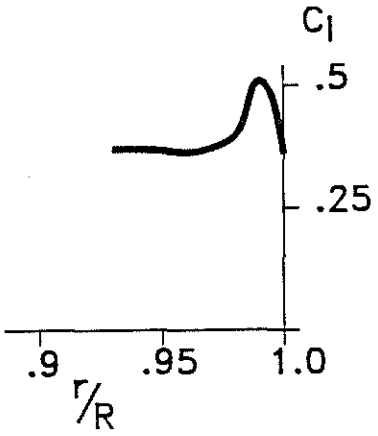

Figure 3: measured tip load on a model rotor in hover (ref. 2).

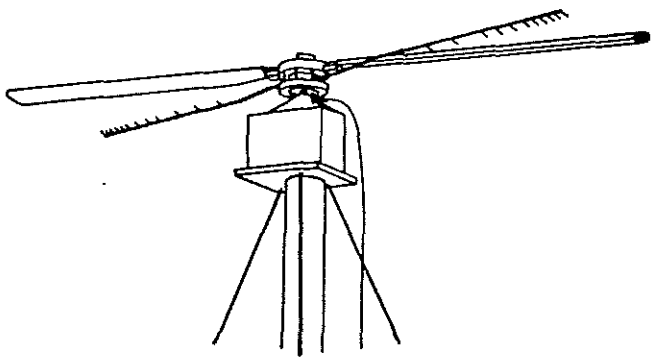

Figure 4: the model with the co-rotating rake for total pressure measurements.

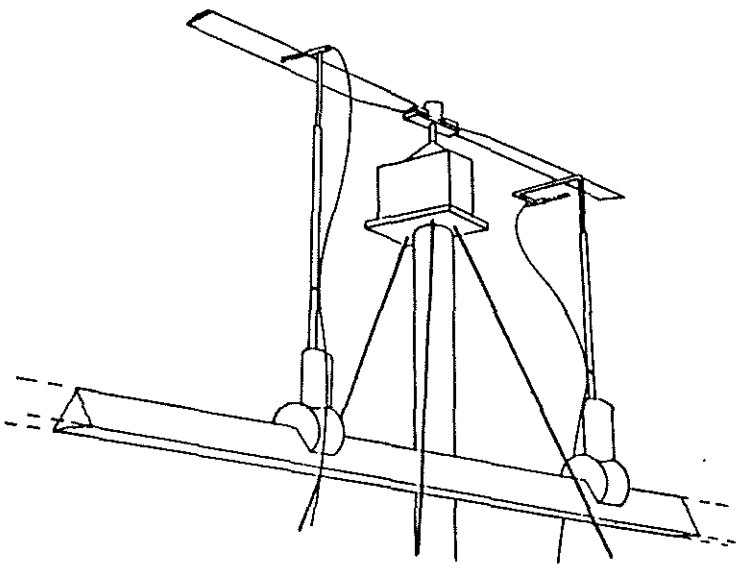

Figure 5: the position of the hot wires.

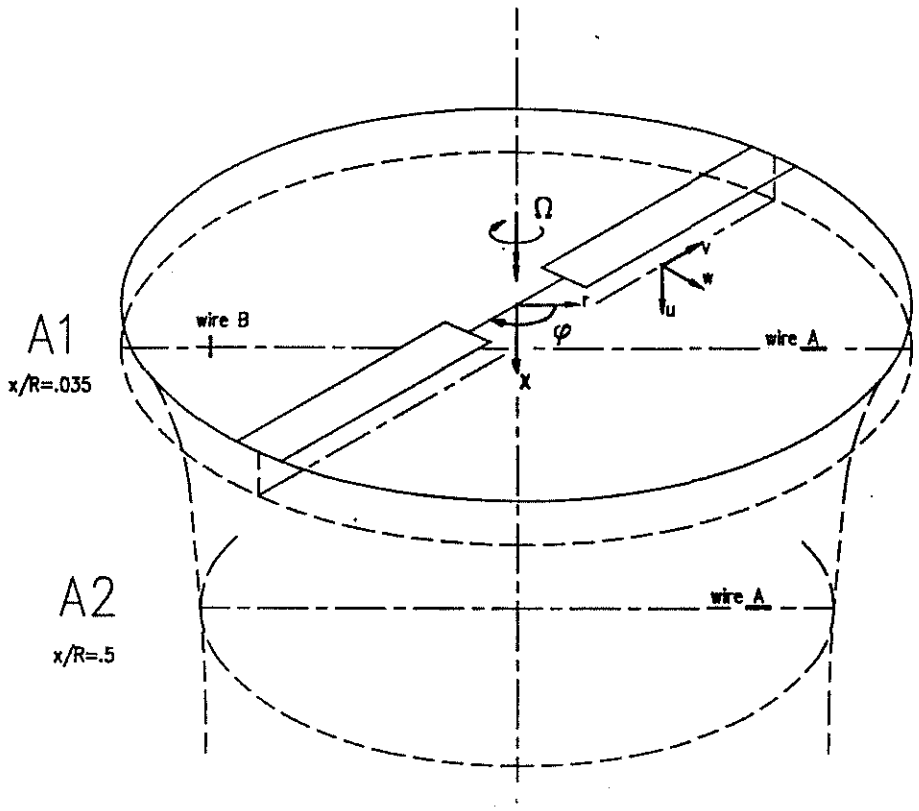

Figure 6: survey of notations and sign conventions.

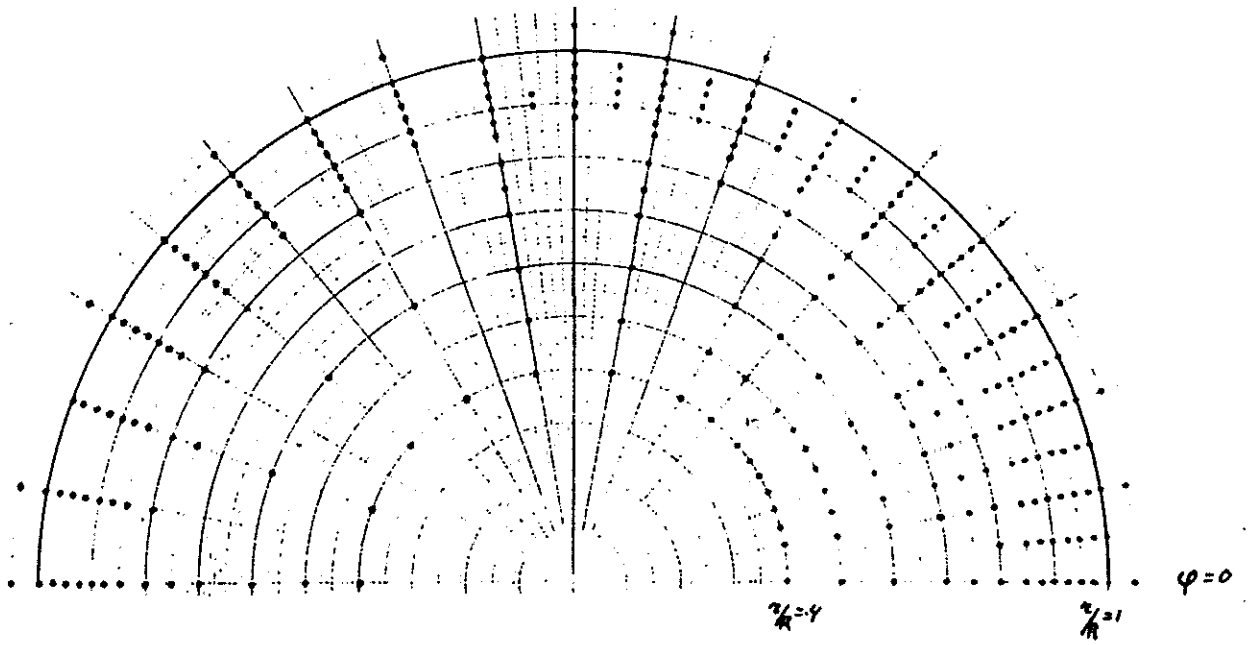

Figure 7: the rotating rake data points; at the 'missing' positions in the grid, interpolated data have been used.

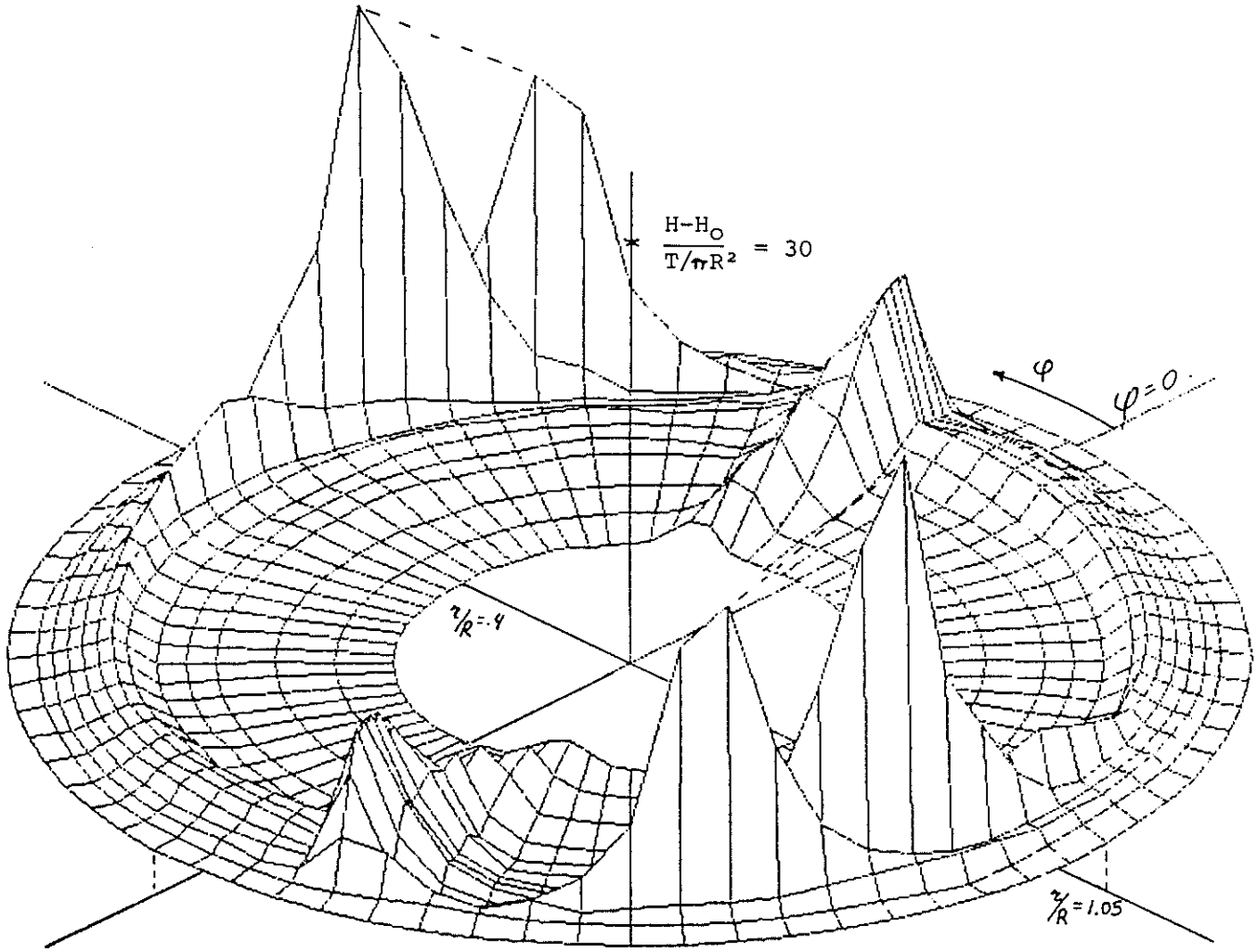

Figure 8: the distribution of $(H-H_0)_r$ in plane A1 (x/R = 0.035) shown in rotating system coordinates. ϕ = 0 and π are the blade positions. The data for ϕ and $\phi + \pi$ are equal as they have been averaged. The r,ϕ grid is the grid of figure 7.

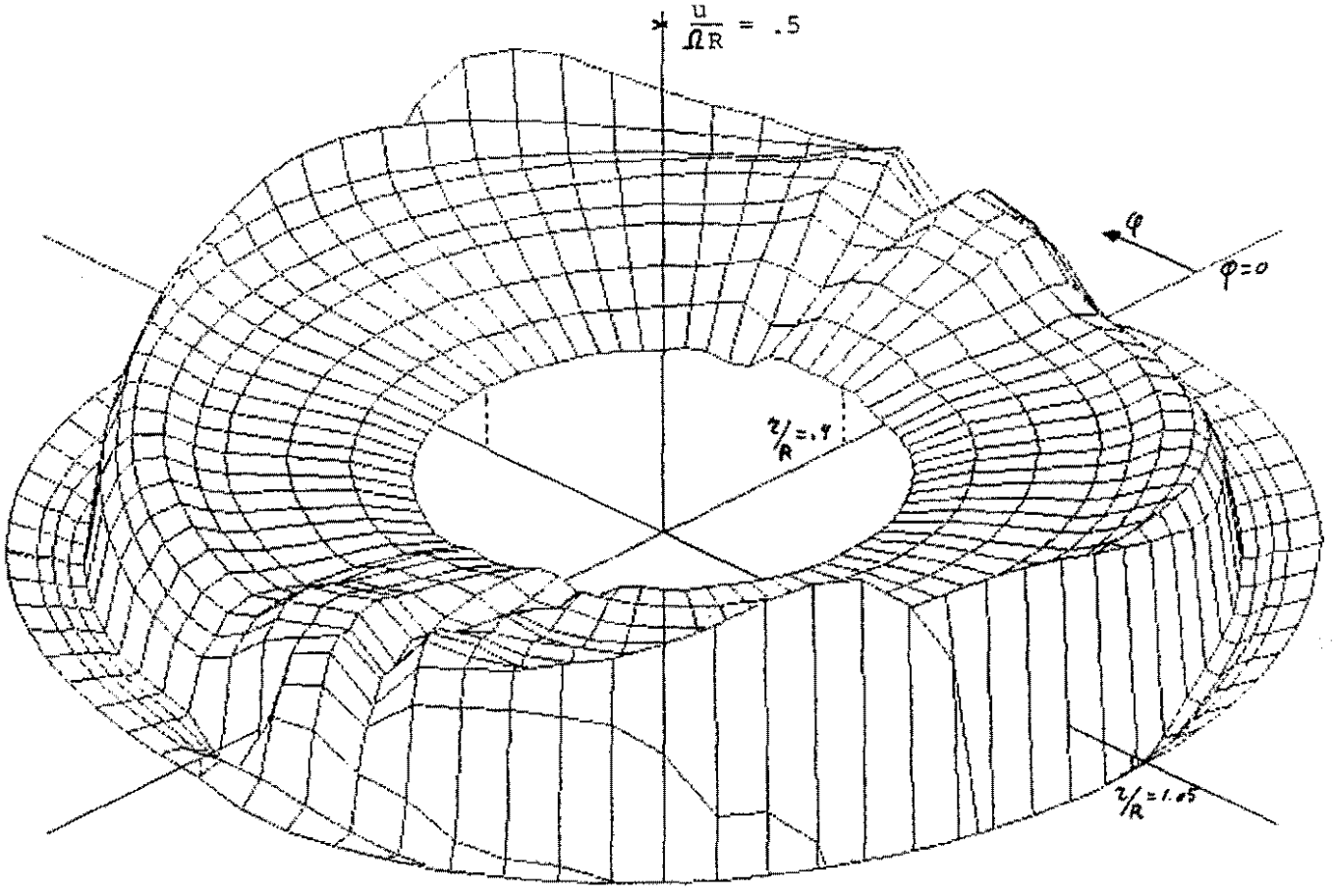

Figure 9: the distribution of the axial velocity u. Explanation as in figure 8.

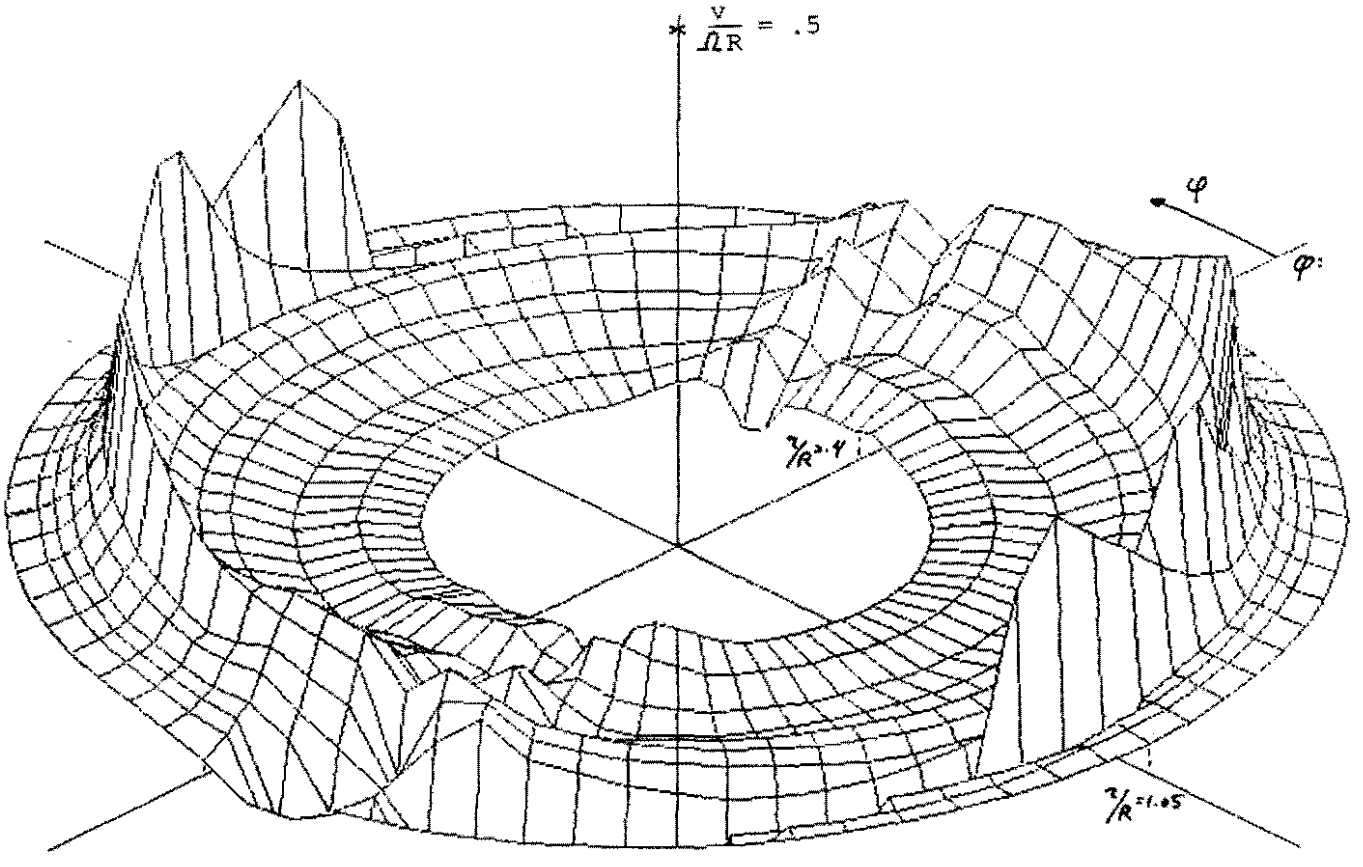

Figure 10: the distribution of the radial velocity v. Explanation as in fig. 8.

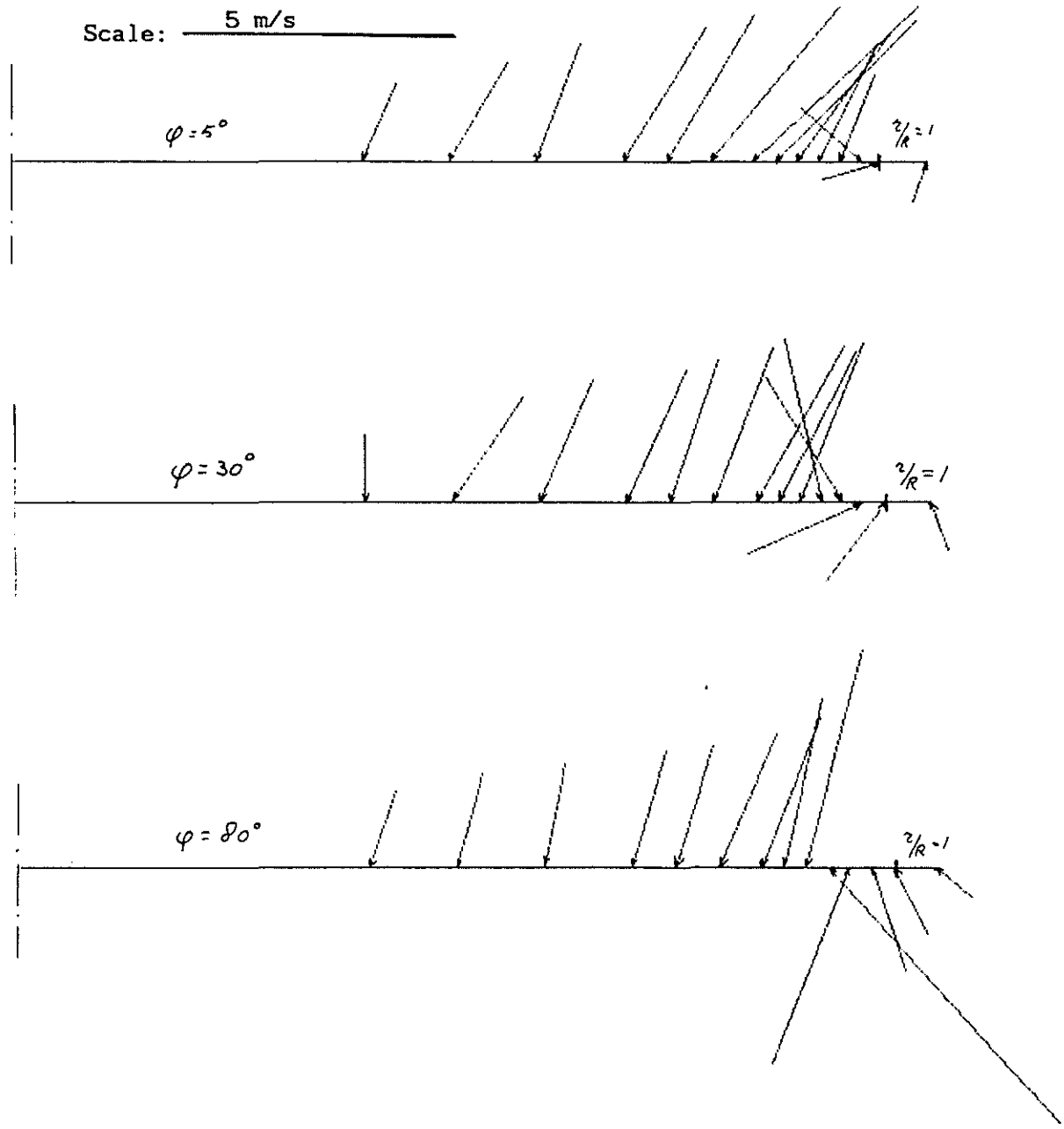

Figure 11: vectorial presentation of u and v for several azimuthal positions in plane A1.

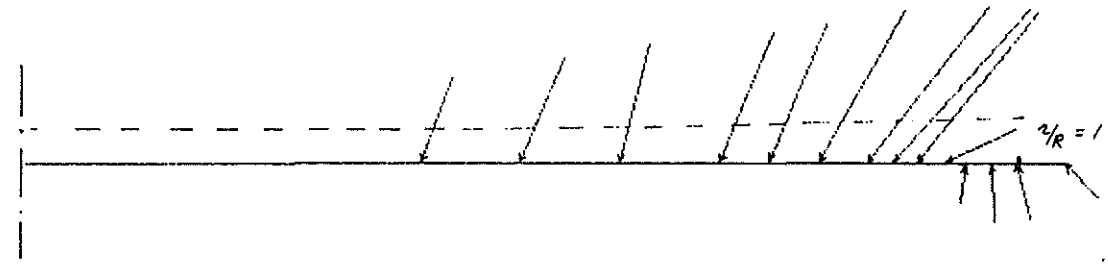

Figure 12: vectorial presentation of the average velocity in plane A1. The dashed line is the rotor blade position.

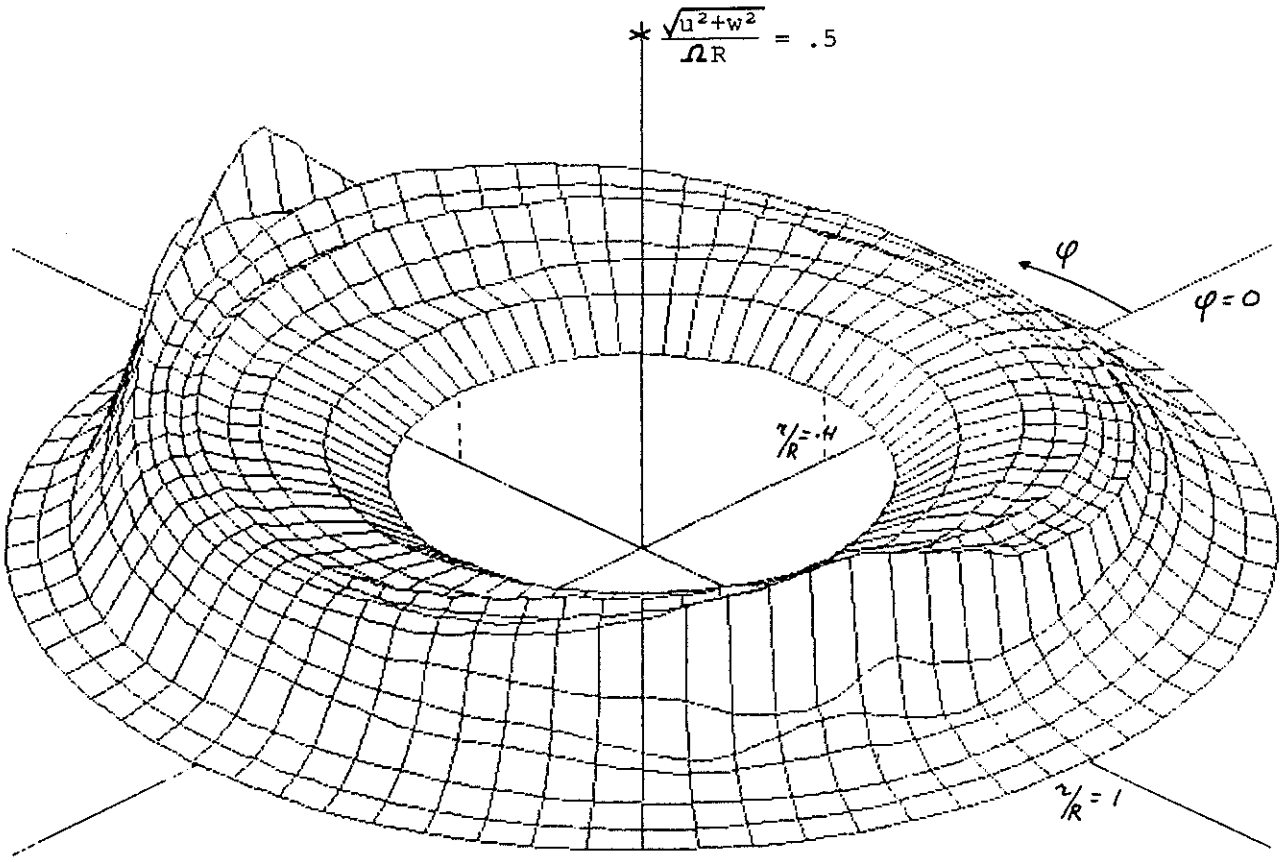

Figure 13: the distribution $\sqrt{u^2 + w^2}$ in plane A2 (x/R = .5), shown in rotating system coordinates. The data for ϕ and $\phi + \pi$ are <u>not</u> averaged: the picture shows data for $0 \leq \phi \leq 2\pi$.